# Electrical tuning of skyrmion dynamics in multiferroic composite thin films

Dongxing Yu,[1] Shutian Luo,[1] Yaojin Li,[1] Vladimir Koval,[2] and Chenglong Jia[1,3,*]

[1]*Key Laboratory for Magnetism and Magnetic Materials of MOE, Lanzhou University, 730000 Lanzhou, China*

[2]*Institute of Materials Research, Slovak Academy of Sciences, Watsonova 47, 04001 Kosice, Slovakia*

[3]*Institut für Physik, Martin-Luther Universität Halle-Wittenberg, 06099 Halle (Saale), Germany*

(Received 11 June 2019; revised manuscript received 5 August 2019; published 5 September 2019)

A lack of space-inversion symmetry along with broken time-reversal symmetry at ferromagnetic/ferroelectric interfaces gives rise to the electric field control of the effective magnetic field and the Dzyaloshinskii-Moriya interaction, thus allowing for the formation of multiferroic skyrmions at room temperature. The electric-field-driven evolution of spin textures at the ferromagnetic/ferroelectric interface is investigated by means of Monte Carlo simulations. It is demonstrated that the skyrmion lattice can be stabilized by the moderate interfacial magnetoelectric couplings. The chirality, radius, position, and numbers of skyrmions are found to be tunable by an external the electric field. The nonequilibrium dynamics of skyrmions, however, strongly depends on the frequency of the applied time-oscillating electric field. With the increase of the frequency of the ac electric field, multiferroic skyrmions become unstable and after several periods they are, ultimately, damping down to the helimagnetic phase. Under microwavelike electric fields, the dynamic multiferroic response of the skyrmion lattice is anisotropic and inhomogeneous. The electric-field-induced resonance spectrum of the magnetic skyrmion with a distinct peak in the imaginary part of permeability is successfully simulated by the Fourier transformation of magnetization.

DOI: 10.1103/PhysRevB.100.104410

## I. INTRODUCTION

The magnetic skyrmion [1,2], a vortex-like spin-swirling texture of topological origin, is of great interest to future spintronic technology because of its numerous advantages, such as nanoscale size [3,4], topologically protected stability [5], and ultra-low power consumption [4,6]. So far, magnetic skyrmions have been observed mainly in metallic chiral B20 structures [7], in which the skyrmion can be efficiently driven by an electric current via spin-transfer torques [7–10]. The skyrmion phase in insulating oxides was discovered in 2012, namely, in the chiral-lattice magnet of $Cu_2OSeO_3$ [11]. The intrinsic magnetoelectric (ME) coupling in $Cu_2OSeO_3$ offers the possibility of manipulation of the skyrmion by an external electric field rather than electric current, which holds a great advantage not only because of a significant reduction in energy consumption (without Joule-heating energy loss), but also due to the added nonvolatile functionality. However, $Cu_2OSeO_3$, as a single-phase multiferroic, is far from its application in spintronic devices due to a low multiferroic transition temperature and a weak magnetoelectric response [12,13]. Therefore, the search for multiferroic skyrmions with strong ME interaction at room temperature is highly desirable.

Theoretically, it is suggested that the competition between the symmetric $(\mathbf{M}_i \cdot \mathbf{M}_j)$-like exchange interaction (here $\mathbf{M}_i$ and $\mathbf{M}_j$ are spins on neighboring sites) and the asymmetric $(\mathbf{M}_i \times \mathbf{M}_j)$-like Dzyaloshinskii-Moriya interaction (DMI) [14,15] is the key ingredient for the formation of the magnetic skyrmion in chiral-lattice magnets. In addition, magnetic field $\mathbf{H}$ is found to play a substantial role in manipulating the skyrmion structure and its dynamics [16–18]. In this work, we show that all these phenomena can find their analogies in the coupled ferromagnetic/ferroelectric (FM/FE) heterostructures. Furthermore, the interfacial ME effects can enable the formation of multiferroic skyrmions at room temperature, and they may give rise to a number of internal dynamic modes of the skyrmion by applying the time-oscillating electric fields. The skyrmion dynamic modes include the uniform breathing, the chirality reversal, and the coherent displacements of the skyrmion lattice, which are often accompanied by skyrmion annihilation and re-creation. Under small microwave-like electric fields, the multiferroic dynamics of the skyrmion lattice can be characterized by an anisotropic ME response. The resonant frequency is simulated in the work by tuning the frequency of the applied electric fields. These findings demonstrate the feasibility of using the ac electric field for the controllable manipulation of skyrmions at the FM/FE interfaces.

## II. INTERFACIAL MAGNETOELECTRIC EFFECTS

The asymmetric DMI requires a broken space-inversion symmetry and spin-orbit coupling. The FM/FE interfaces are an excellent candidate for realization of the multiferroic DMI since their structure-inversion symmetry is naturally broken and an interfacial spin-orbit coupling of the Rashba type additionally exists due to the electrostatic potential difference at the interface [19],

$$\mathcal{F}_{SO} = \alpha(\mathbf{k} \times \hat{\mathbf{e}}_z) \cdot \mathbf{s}, \quad (1)$$

*cljia@lzu.edu.cn

 

where $\mathbf{k}$ is the momentum of electrons, $\mathbf{s}$ is the Pauli's spin matrices, and $\hat{\mathbf{e}}_z$ is the unit vector normal to the interface. The strength of the Rashba spin-orbit interaction (RSOI) $\alpha$ is determined by the surface potential gradient $\nabla_z V(r)$, thus it can be tuned by changing the shape of the interfacial confining potential using an external electric field [20]. If a ferromagnetic metal is attached with the gate polarized electric dipole moments, the electric field modulation can be substantially enhanced at the interface due to the large interface screening that linearly depends on the normal component of the FE polarization [21–23]. Based on a Rashba band [24], the indirect DMI mediated by spin-polarized conduction electrons in FM metal occurs at the interface owing to the presence of RSOI, which brings together the spin and the real space (the lattice). The strength of the DMI is reported to be a linear function of the strength of the RSOI $\alpha$, and so is the FE polarization in the FE systems. Together with the tight-binding model, in which the DMI is mediated by conduction electrons and relies on the existence of high spin-orbit heavy-metal atoms of the adjacent layer [4,25], the asymmetric exchange interaction at the FM/FE interface can be, in general, written as

$$\mathcal{F}_{\mathrm{DMI}} = \sum_{\mathrm{i,j}} \mathbf{D}_{\mathrm{ij}} \cdot (\mathbf{M}_{\mathrm{i}} \times \mathbf{M}_{\mathrm{j}}) \tag{2}$$

with $\mathbf{D}_{\mathrm{ij}} = (\mathbf{D}^0_{\mathrm{ij}} + \mathbf{D}^{\mathrm{P}}_{\mathrm{ij}})$, where $\mathbf{D}^0_{\mathrm{ij}}$ is assumed to originate from the interaction between transition metal atoms and heavy element impurities and is insensitive to the applied electric field. $\mathbf{D}^{\mathrm{P}}_{\mathrm{ij}}$, however, varies with the FE polarization $P_z$ linearly. As for the direction of the DMI, it is shown that both $\mathbf{D}^0_{\mathrm{ij}}$ and $\mathbf{D}^{\mathrm{P}}_{\mathrm{ij}}$ are all perpendicular to the unit vector $\mathbf{r}_{\mathrm{ij}}$ between $\mathbf{M}_{\mathrm{i}}$ and $\mathbf{M}_{\mathrm{j}}$ and lie in the interface plane, i.e., $\mathbf{D}_{\mathrm{ij}} \sim (\mathbf{r}_{\mathrm{ij}} \times \hat{\mathbf{e}}_z)$.

On the other hand, the FM/FE interface with intrinsically broken space-inversion symmetry and time-reversal symmetry is suggested to exhibit a ME coupling restricted to the nanometer-sized region of near-interface [26–28],

$$\mathcal{F}_{\mathrm{ME}} = \gamma \langle \mathbf{P} \rangle \cdot \mathbf{M} - \tfrac{3}{2}\lambda\sigma \cos^2\phi. \tag{3}$$

The first $\gamma$ term takes its origin from a nonuniform, interfacial spin density coupled to the ferroelectric polarization due to the spin-dependent surface screening in the vicinity of the spin-diffusion length [29–31]. $\gamma$ is the coupling strength in units of s/F. Below terahertz and with the spin-diffusion length being around tens of nanometers in transition metals [32], the linear direct magntoelectric coupling is assumed to involve all magnetic moments in the present ultrathin FM film (∼5 nm), where variations along the interface normal are neglected. The second $\lambda$ term involves piezoelectricity and the magnetostriction at the interface, associated with an additional voltage-controlled uniaxial anisotropy energy for the FM layer [28,33,34]. $\lambda$ is the average magnetostriction coefficient, and $\phi$ is the angle between the magnetization $\mathbf{M} = \sum_{\mathrm{i}} \mathbf{M}_{\mathrm{i}}/N_{\mathrm{FM}}$ and the direction of the stress $\boldsymbol{\sigma}$ across the interface. From Eq. (3), the ME coupling can result in an effective magnetic field

$$H_{\mathrm{ME}} = -\delta F_{\mathrm{ME}}/\delta \mathbf{M}, \tag{4}$$

which directly responds to the applied external electric field.

The aforementioned description of the multiferroic properties at the FM/FE interface allows for the formulation of conditions for the ferroelectric tuning of both the asymmetric DMI [Eq. (2)] and the effective magnetic field [Eq. (4)] in the skyrmion phase. The possibility of manipulation of the magnetic skyrmion by an external electric field at room temperature makes these vortex-like structures a potential candidate for spintronic applications.

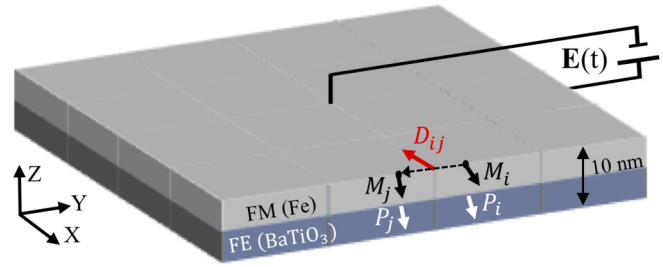


FIG. 1. A schematic of the FM/FE heterostructure. The epitaxially grown multiferroic heterostructure in a coarse-grained approach consists of $N_{\mathrm{FE}} = N_{\mathrm{FM}} = 21 \times 21$ electric dipole moments $\mathbf{P}_{\mathrm{i}}$ (white arrows) and magnetic moments $\mathbf{M}_{\mathrm{i}}$ (black arrows), respectively. The interfacial DMI, $\mathbf{D}_{\mathrm{ij}} \sim (\mathbf{r}_{\mathrm{ij}} \times \hat{\mathbf{e}}_z)$ (red arrow), lies in the interface plane. $\mathbf{E}(t)$ is an applied (time-oscillating) electric field normal to the interface.

## III. SIMULATIONS OF SKYRMION DYNAMICS

In the present study, the electric-field-driven magnetic dynamics of a two-dimensional FM/FE bilayer structure is investigated by means of Monte Carlo simulations [35]. We choose Fe and $BaTiO_3$ as the candidates for FM and FE subsystems, respectively. From a computational point of view, without loss of general physical properties, the coarse-graining with cell size $a = 5$ nm is conveniently used to obtain the quantities of polarization $\mathbf{P}$ and magnetization $\mathbf{M}$ [36]. Calculations are mostly carried out for $N_{\mathrm{FM}} = N_{\mathrm{FE}} = 21 \times 21$ classical (three-dimensional) electric dipole moment $\mathbf{P}_{\mathrm{i}}$ and magnetic moment $\mathbf{M}_{\mathrm{j}}$ (cf. Fig. 1).

For the FE layer, the elastic Gibbs function $F_{\mathrm{FE}}$ corresponding to the tetragonal phase of $BaTiO_3$ film reads [28]

$$\begin{aligned} F_{\mathrm{FE}} = &-\frac{\alpha}{2}\sum_{\mathrm{i}} \mathbf{P}_{\mathrm{i}}^2 + \frac{\beta}{4}\sum_{\mathrm{i}} \mathbf{P}_{\mathrm{i}}^4 + \kappa \sum_{\langle \mathrm{ij} \rangle} (\mathbf{P}_{\mathrm{i}} - \mathbf{P}_{\mathrm{j}})^2 \\ &+ c_{\mathrm{eff}} u_1 \sum_{\mathrm{i}} P_{\mathrm{iz}} + \frac{N_{\mathrm{FE}}}{2} C_{\mathrm{u}} u_1^2 - \sum_{\mathrm{i}} \mathbf{E} \cdot \mathbf{P}_{\mathrm{i}}. \end{aligned} \tag{5}$$

Here, $c_{\mathrm{eff}} = 2c_{31} - c_{33}/n$ with $c_{3\xi} = \partial P_z/\partial u_\xi$ $(\xi = 1, 2, 3)$ being the improper piezoelectric tensor of the FE film. The symmetry $c_{31} = c_{32}$ is considered in order to derive the effective piezoelectric constant $c_{\mathrm{eff}}$ [37]. It should be noted that, for epitaxially strained FE films, the strain components satisfy $u_4 = u_5 = u_6 = 0$, $u_1 = u_2 \neq 0$, and the strain perpendicular to the interface is determined by the Poisson ratio $n = -u_1/u_3$. $\mathbf{E}$ is the external electric field and $C_{\mathrm{u}}$ is the stiffness coefficient of the FE. For the FM layer, the energy density can be expressed by $F_{\mathrm{FM}} = F_{\mathrm{XC}} + F_{\mathrm{DMI}}$ with

$$F_{\mathrm{XC}} = -\frac{A}{a^2 M_{\mathrm{s}}^2} \sum_{\langle \mathrm{ij} \rangle} \mathbf{M}_{\mathrm{i}} \cdot \mathbf{M}_{\mathrm{j}} - \frac{K_1}{M_{\mathrm{s}}^2} \sum_{\mathrm{i}} M_{\mathrm{iz}}^2, \tag{6}$$

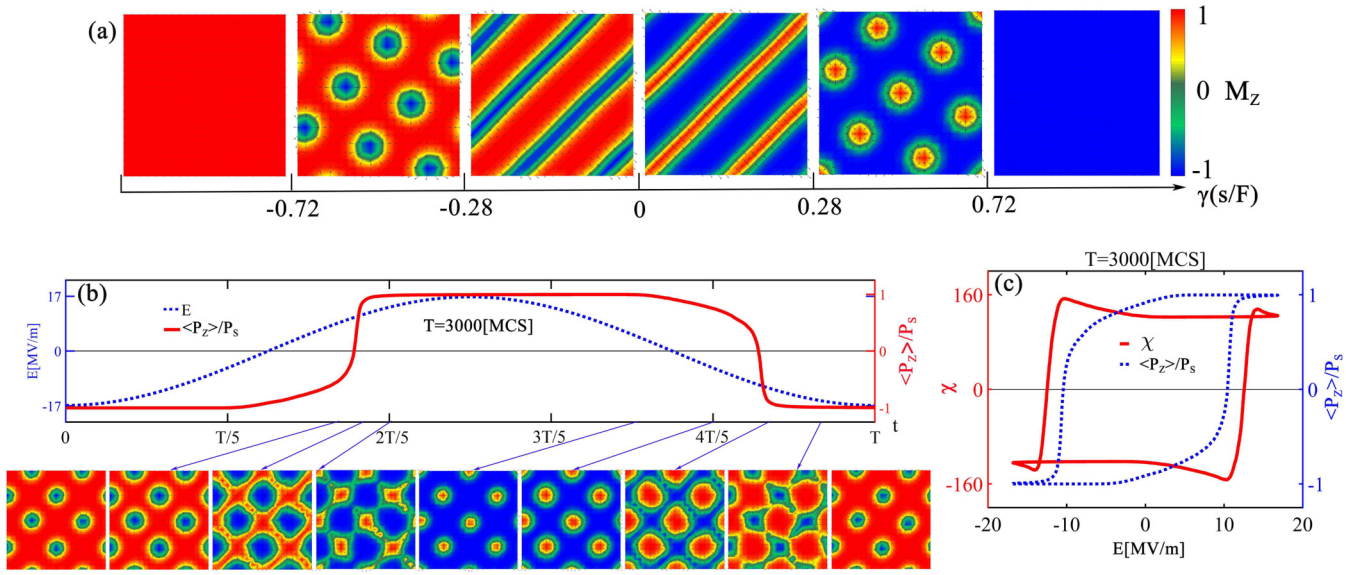


FIG. 2. (a) Phase diagram as a function of the ME coupling strength $\gamma$. The color and arrows denote the vertical components and directions of the magnetization, respectively. (b) Time evolution of skyrmions and FE polarization (red line) under an ac electric field with the period $T = 3000$ MCS and the ME coupling $\gamma = 0.55$ s/F. Snapshots show, respectively, the instantaneous spin configurations at time: $t = 0$, 1000, 1100, 1200, 2100, 2400, 2600, 2700, and 3000 MCS. (c) The corresponding hysteresis loops of the total chirality $\chi$ (red line) and average polarization $\langle P_z\rangle/P_s$ (blue dashed line).

where $M_s$, $A$, and $K_1$ are, respectively, the saturation magnetization, the nearest-neighbor exchange interaction, and the magnetocrystalline anisotropy constant with the easy axis perpendicular to the interface.

The multiferroic dynamics of the electric dipole moment $\mathbf{P}_i$ and the magnetic moment $\mathbf{M}_j$ is governed by the total free energy $F = F_{FE} + F_{FM} + F_{ME}$. The material parameters for the FE layer are chosen as $\alpha = 2.77 \times 10^7$ V m/C [38], $\beta = 1.70 \times 10^8$ V m$^5$/C$^3$, [38] $\kappa = 1.0 \times 10^8$ V m/C [39], and $P_s = 0.27$ C/m$^2$. Here, $C_u = 3.90 \times 10^9$ N/m$^2$ is used to reproduce the lattice mismatch ($\sim$1.4%) between the bcc Fe[001] film and the tetragonal $BaTiO_3$ at room temperature [40]. The improper piezoelectric constants are set as those of $BaTiO_3$ [37]: $c_{31} = 0.3$ C/m$^2$, $c_{33} = 6.7$ C/m$^2$, and the Poisson ratio $n = 0.64$ [41]. Further parameters of the FM (iron) layer are $\lambda = 2.07 \times 10^{-5}$ along Fe[100] [33], $A = 2.1 \times 10^{-11}$ J/m [42], $K_1 = 4.8 \times 10^4$ J/m$^3$ [42], and $M_s = 1.71 \times 10^6$ A/m [42]. The induced stress acting on the FM body is given by $\boldsymbol{\sigma} = -C_{11}[u_1, u_2, u_3]$ with the elastic constant $C_{11} = 1.78 \times 10^{11}$ N/m$^2$ of $BaTiO_3$ at the interface [43].

Firstly, the equilibrium spin configurations based on a high-temperature annealing Metropolis algorithm with periodic boundary conditions are investigated in detail [44]. $5 \times 10^4$ Monte Carlo steps (MCS) were used at each temperature of the annealing process. Figure 2(a) shows the ground-state phase diagram as a function of the ME coupling strength $\gamma$. Note that a normal static electric field $\mathbf{E} = (0, 0, E_0)$ with $E_0 = 17$ MV/m is used to obtain a fully electric polarized FE layer. $D_{ij}/J = 1$ with exchange interaction $J = aA$ is used to have enough skyrmions in the limited samples and save the computational cost at the same time. Similarly to the spin textures driven by an external magnetic field in chiral-lattice magnets [45], we found that the helimagnetic phase, the skyrmion lattice phase, and the ferromagnetic phase emerge successively with the increasing strength $\gamma$. The critical values of $\gamma$ are 0.28 and 0.72 s/F, which range in the typical interval of the measured ME coupling strength of coupled FE/FM heterostructures [30,46,47]. This is a very important result, implying that the skyrmion phase would exist even for a relatively weak interfacial ME coupling, for instance in real materials with a smaller value of DMI, once the condition $0.2\frac{D^2}{J} < |\gamma P_s| < 0.8\frac{D^2}{J}$ is satisfied.

Secondly, a time-dependent oscillating electric field $\mathbf{E}(t) = (0, 0, -E_0 \cos \omega t)$ is applied to explore the nonequilibrium behavior of the skyrmion dynamics via the kinetic Monte Carlo method. The initial (nearly perfect) skyrmion lattice with the ME coupling $\gamma = 0.55$ s/F is prepared via the annealing procedure. At the first step of our numerical calculations, the DMI is assumed to be independent of the applied electric field (the effects of the field-dependent DMI will be demonstrated in Fig. 5). Following the reference [44], we define a local chirality $\chi_{\mathbf{r}}$ at the lattice site $\mathbf{r}$ as

$$\chi_{\mathbf{r}} = \mathbf{M}_{\mathbf{r}} \cdot (\mathbf{M}_{\mathbf{r}+\hat{\mathbf{x}}} \times \mathbf{M}_{\mathbf{r}+\hat{\mathbf{y}}}) + \mathbf{M}_{\mathbf{r}} \cdot (\mathbf{M}_{\mathbf{r}-\hat{\mathbf{x}}} \times \mathbf{M}_{\mathbf{r}-\hat{\mathbf{y}}}). \quad (7)$$

For a single localized skyrmion, $|\sum_{\mathbf{r}} \chi_{\mathbf{r}}|$ is equal to unity in the continuum limit. Therefore, the value of the total chirality $\chi = \sum_{\mathbf{r}} \chi_{\mathbf{r}}$ of the FM layer can determine the number and the topological charge of skyrmions. As demonstrated in Figs. 2(b) and 3, the FE layer possesses a typical ferroelectric hysteresislike behavior under the ac electric field [cf. also the P-E loop in Fig. 2(c)]. The skyrmion dynamics, however, does depend on the frequency of the applied electric fields. Under a slowly changing electric field with long period, the magnetic dynamics can adiabatically follow the effective ME field determined by the FE polarization. The periodic changes of the skyrmion lattice and the hysteresis loop of $\chi$-E are shown in Figs. 2(b) and 2(c), respectively. One can see that the dramatic change of skyrmions happens within the narrow

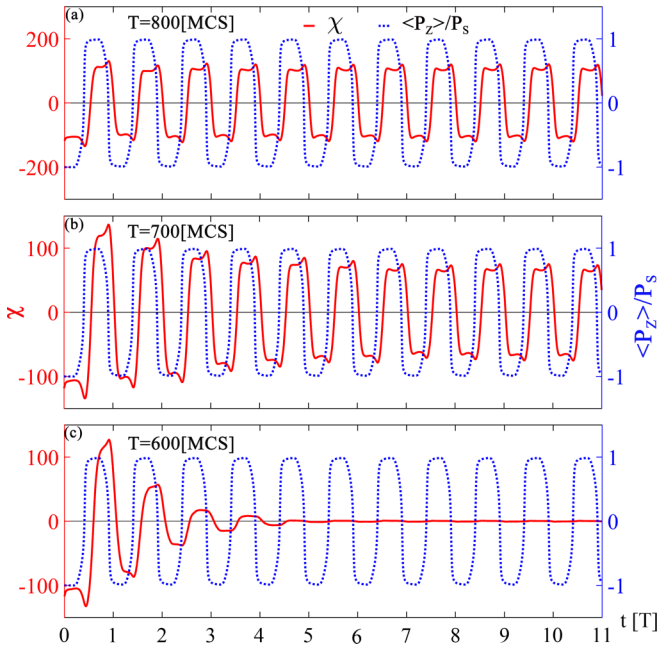


FIG. 3. The total chirality $\chi$ (red line) and the average polarization $\langle P_z\rangle/P_s$ (blue dashed line) as a function of time in the presence of time-oscillating electric field with the periods (a) 800, (b) 700, and (c) 600 MCS.

range of the FE polarization reversal process. Interestingly, during the switching process, the onset nucleation of skyrmion reversal accompanied with coherent periodic displacements of the skyrmion lattice is observed, as demonstrated in the snapshots of the dynamic process of electrical skyrmion annihilation and creation in Fig. 2(b). However, the skyrmion lattice becomes unstable with increasing the frequency of the ac electric field (cf. Fig. 3). The simulated critical frequency is about $\omega = 2\pi/600$ MCS$^{-1}$. Above this frequency, the damping of skyrmions becomes fast and after several periods the skyrmions eventually melt into the helimagnetic phase.

For a more complete scenario of the skyrmion dynamics, a single skyrmion is generated with the open boundary condition. Differently from the skyrmion lattice, the single skyrmion is confined at the center of the FM layer. Figure 4 presents the time evolution of the single skyrmion with the same ME coupling strength $\gamma$ as that used in the periodic boundary conditions. A uniform breathing mode rather than the nucleation of skyrmion reversal is driven by the time-dependent electric field with longer period $T = 6000$ MCS.

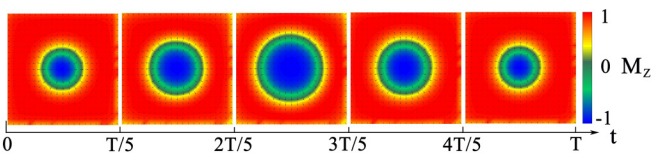


FIG. 4. Snapshots of simulatd dynamics of a single skyrmion within one period $T$. Here, $D_{ij}/J = 0.35$, the period of ac electric field $T = 6000$ MCS, and the open boundary condition are used during the numerical calculations.

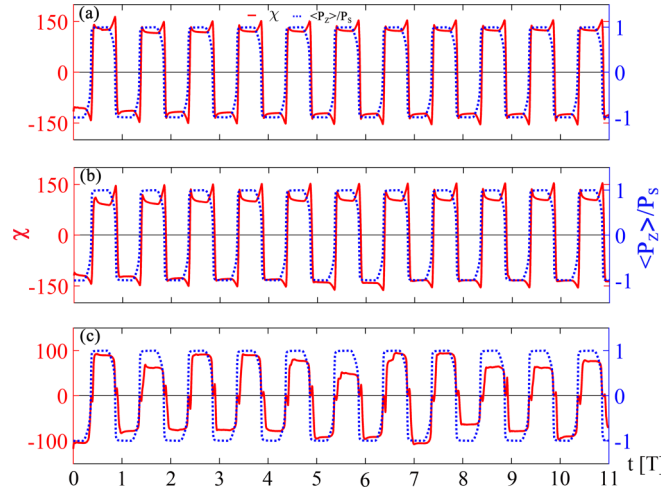


FIG. 5. Dynamic process of $\chi$ (red line) and $\langle P_z\rangle/P_s$ (blue dashed line) under the polarization-dependent DMI: (a) $D_{ij} = D_0$, (b) $D_{ij} = D_0 + 0.1D_0\langle P_z(t)\rangle/P_s$, and (c) $D_{ij} = D_0\langle P_z(t)\rangle/P_s$. Here the period of applied ac electric field $T = 3000$ MCS, the ME coupling $\gamma = 0.55$ s/F, and DMI $D_0/J = 0.99$.

Now, we will explore the effects of the ferroelectric tunable DMI relating to the RSOI at the interface. For comparison, the numerical simulations are carried out with (i) $D_{ij} = D_0$, (ii) $D_{ij} = D_0 + 0.1\frac{\langle P_z(t)\rangle}{P_s}D_0$, and (iii) $D_{ij} = \frac{\langle P_z(t)\rangle}{P_s}D_0$ (note that other parameters are the same). It is interesting that, except for the values of chirality, the overall behavior of skyrmion dynamics is very similar in all the three cases, as shown in Fig. 5. This implies that the skyrimion dynamics is mostly dominated by the effective Zeeman field. However, DMI is essential to formation of the multiferroic skyrmion in FE/FM interfaces.

Experimentally, the magnetic permeability is usually measured to study the response of a material subjected to an applied ac magnetic field [48,49]. In the present study, we show that the magnetic dynamics can be driven by an external electric field via the interfacial ME coupling as well. Therefore, it would be interesting to see how the skyrmions are excited by applying small *transverse* ac electric fields under a large static electric field. Such dynamic multiferroic response of the skyrmion lattice is numerically investigated under the time-varying electric fields, $\mathbf{E}(t) = E_z\hat{\mathbf{e}}_z + E_x\cos\omega t\,\hat{\mathbf{e}}_x$, and is characterized by a spatially resolved tensor, $\mu_{\xi x} = \delta\mathbf{M}^{\xi}_{\mathbf{r}}(t)/E_x$, which is termed as the magnetoelectric permeability. As demonstrated in Figs. 6(b) and 6(c), the anisotropic magnetoelectric permeability occurs in the system; the half-moon-like pattern and circle-like pattern of $\mathrm{Re}(\mu_{xx})$ and $\mathrm{Re}(\mu_{zx})$, respectively, are clearly observed. It is found that the center region of each skyrmion exhibits a relatively weaker electromagnetic response than the outer region, when the ferroelectric polarization of the FE layer is not perfectly excited along the $x$ axis. Furthermore, as indicated in ferromagnetic resonance dynamics excited by the microwave electric field, the energy of the ac field can be effectively absorbed by tuning of the frequency of the ac field to the resonant frequency of the system. A noticeable peak at the imaginary part of magnetic permeability $\mathrm{Im}(\mu_{zx})$ is

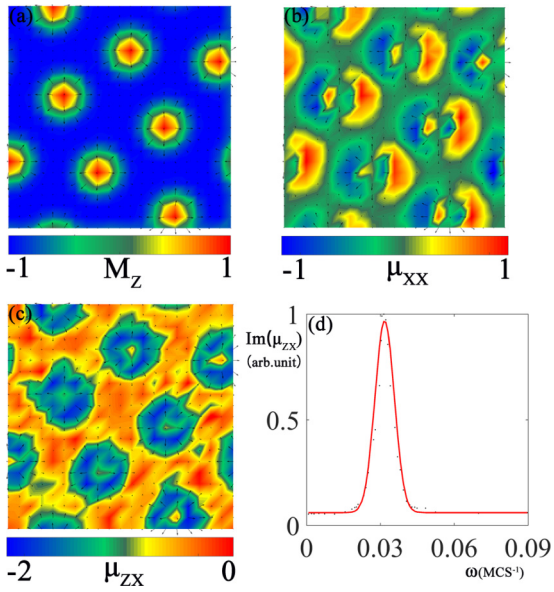


FIG. 6. (a) The prepared (initial) skyrmion lattice for dynamic multiferroic response. (b) and (c) are, respectively, snapshotted patterns of the real parts $\mathrm{Re}(\mu_{xx})$ and $\mathrm{Re}(\mu_{zx})$ of magnetoelectric permeability at constant frequency $\omega = 0.002\ \mathrm{MCS}^{-1}$. (d) Imaginary part of the permeability $\mathrm{Im}\mu_{zx}$ vs the frequency of applied ac electric field. Here, the applied time-varying electric filed reads $\mathbf{E}(t) = E_z\hat{\mathbf{e}}_z + E_x \cos\omega t\, \hat{\mathbf{e}}_x$ with $E_z = 17\ \mathrm{MV/m}$ and $E_x = E_z/10$.

clearly observed in Fig. 6(c), which displays the $z$-direction absorption spectra calculated from the Fourier transformation of magnetization $\mathbf{M}(t) = (1/N_{\mathrm{FM}})\sum_{\mathbf{r}} \mathbf{M}_{\mathbf{r}}(t)$. The resonant frequency is about $\sim$0.031 $\mathrm{MCS}^{-1}$. This dynamic multiferroic response of the coupled FE/FM composites upon excitation by the microwave electric field provides an alternative approach for probing the skyrmion lattice. In and above the gigahertz range, the spin-wave spectra and a frequency-dependent ME coupling should be considered. Therefore, the dynamic response of multiferroic skyrmions needs to be further investigated in order to better understand their complex behavior.

## IV. CONCLUSION

In the present work, the effects of the interfacial ME coupling on spin textures at the FM/FE interface were theoretically analyzed. The linear dependence of the Rashba spin-orbit interaction, asymmetric DMI, and effective magnetic field driven by the FE polarization are shown to bring about the multiferroic skyrmion phase at room temperature. By applying the time-dependent electric field, the nonequilibrium evolution and resonance behavior of the skyrmion dynamics were successfully simulated on the basis of the Monte Carlo method. Several internal modes, such as nucleation of chirality reversal, uniform breathing, annihilation, and recreation of the multiferroic skyrmion, were found to exist during the dynamical evolution processes. The resonant frequency and damping phenomena of the skyrmion lattice under ac electric fields are discussed accordingly. Our model simulation successfully describes the nature, in particular, the dynamic multiferroic response of skyrmions at FM/FE interfaces, and gives a pathway for the ultralow power manipulation of these skyrmions using the moderate electric fields at room temperature.

## ACKNOWLEDGMENTS

This work is supported by the National Natural Science Foundation of China (Grants No. 11474138 and No. 11834005), the German Research Foundation (Grant No. SFB 762), the Program for Changjiang Scholars and Innovative Research Team in University (Grant No. IRT-16R35), Ministry of Science and Technology of China through Grant No. CN-SK-8-4, the Slovak Academy of Sciences (Grant No. 2/0059/17), and the Slovak Research and Development Agency (APVV SK-CN-2017-0004).

[1] U. K. Rößler, A. N. Bogdanov, and C. Pfleiderer, Spontaneous skyrmion ground states in magnetic metals, Nature (London) **442**, 797 (2006).

[2] S. Mühlbauer, B. Binz, F. Jonietz, C. Pfleiderer, A. Rosch, A. Neubauer, R. Georgii, and P. Böni, Skyrmion lattice in a chiral magnet, Science **323**, 915 (2009).

[3] N. Romming, C. Hanneken, M. Menzel, J. E. Bickel, B. Wolter, Kirsten von Bergmann, A. Kubetzka, and R. Wiesendanger, Writing and deleting single magnetic skyrmions, Science **341**, 636 (2013).

[4] A. Fert, V. Cros, and J. Sampaio, Skyrmions on the track, Nat. Nanotechnol. **8**, 152 (2013).

[5] X. Z. Yu, N. Kanazawa, Y. Onose, K. Kimoto, W. Z. Zhang, S. Ishiwata, Y. Matsui, and Y. Tokura, Near room-temperature formation of a skyrmion crystal in thin-films of the helimagnet FeGe, Nat. Mater. **10**, 106 (2011).

[6] T. Schulz, R. Ritz, A. Bauer, M. Halder, M. Wagner, C. Franz, C. Pfleiderer, K. Everschor, M. Garst, and A. Rosch, Emergent electrodynamics of skyrmions in a chiral magnet, Nat. Phys. **8**, 301-304 (2012).

[7] N. Nagaosa and Y. Tokura, Topological properties and dynamics of magnetic skyrmions, Nat. Nanotechnol. **8**, 899 (2013).

[8] F. Jonietz, S. Mühlbauer, C. Pfleiderer, A. Neubauer, W. Münzer, A. Bauer, T. Adams, R. Georgii, P. Böni, and R. A. Duine *et al.*, Spin transfer torques in MnSi at ultralow current densities, Science **330**, 1648 (2010).

[9] X. Z. Yu, N. Kanazawa, W. Z. Zhang, T. Nagai, T. Hara, K. Kimoto, Y. Matsui, Y. Onose, and Y. Tokura, Skyrmion flow near room temperature in an ultralow current density, Nat. Commun. **3**, 988 (2012).

[10] S. Woo, K. Litzius, B. Krüger, MY. Im, L. Caretta, K. Richter, M. Mann, A. Krone, R. M. Reeve, and M. Weigand *et al.*, Observation of room-temperature magnetic skyrmions and their current-driven dynamics in ultrathin metallic ferromagnets, Nat. Mater. **15**, 501 (2016).

[11] S. Seki, X. Yu, S. Ishiwata, and Y. Tokura, Observation of skyrmions in a multiferroic material, Science **336**, 198 (2012).

[12] S. Seki, S. Ishiwata, and Y. Tokura, Magnetoelectric nature of skyrmions in a chiral magnetic insulator $Cu_2OSeO_3$, Phys. Rev. B **86**, 060403(R) (2012).

[13] J.-W. G. Bos and C. V. Colin, and T. T. M. Palstra, Magnetoelectric coupling in the cubic ferrimagnet $Cu_2OSeO_3$, Phys. Rev. B **78**, 094416 (2008).

[14] I. Dzyaloshinsky, A thermodynamic theory of weak ferromagnetism of antiferromagnetics, Phys. Chem. Solids **4**, 241 (1958).

[15] T. Moriya, Anisotropic Superexchange Interaction and Weak Ferromagnetism, Phys. Rev. **120**, 91 (1960).

[16] A. Tonomura, X. Yu, K. Yanagisawa, T. Matsuda, Y. Onose, N. Kanazawa, H. S. Park, and Y. Tokura, Real-space observation of skyrmion lattice in helimagnet MnSi thin samples, Nano Lett. **12**, 1673 (2012).

[17] H. Wilhelm, M. Baenitz, M. Schmidt, U. K. Rößler, A. A. Leonov, and A. N. Bogdanov, Precursor Phenomena at the Magnetic Ordering of the Cubic Helimagnet FeGe, Phys. Rev. Lett. **107**, 127203 (2011).

[18] X. Z. Yu, Y. Onose, N. Kanazawa, J. H. Park, J. H. Han, Y. Matsui, N. Nagaosa, and Y. Tokura, Real-space observation of a two-dimensional skyrmion crystal, Nature (London) **465**, 901 (2010).

[19] E. I. Rashba, Properties of semiconductors with an extremum loop: I. Cyclotron and combinational resonance in a magnetic field perpendicular to the plane, Sov. Phys.-Solid State **2**, 1109 (1960).

[20] M. Heide, G. Bihlmayer, Ph. Mavropoulos, A. Bringer, and S. Blügel, Spin-orbit driven physics at surfaces, Newsletter Psi-K Network **78**, 1 (2006).

[21] D. Di Sante, P. Barone, R. Bertacco, and S. Picozzi, Electric control of the giant Rashba effect in bulk GeTe, Adv. Mater. **25**, 509 (2013).

[22] A. Stroppa, D. Di Sante, P. Barone, M. Bokdam, G. Kresse, C. Franchini, M. H. Whangbo, and S. Picozzi, Tunable ferroelectric polarization and its interplay with spin-orbit coupling in tin iodide perovskites, Nat. Commun. **5**, 5900 (2014).

[23] J. He, D. Di Sante, R. Li, X. Q. Chen, J. M. Rondinelli, and C. Franchini, Tunable metal-insulator transition, Rashba effect and Weyl Fermions in a relativistic charge-ordered ferroelectric oxide, Nat. Commun. **9**, 492 (2018).

[24] A. Kundu and S. Zhang, Dzyaloshinskii-Moriya interaction mediated by spin-polarized band with Rashba spin-orbit coupling, Phys. Rev. B **92**, 094434 (2015).

[25] M. Bode, M. Heide, K. von Bergmann, P. Ferriani, S. Heinze, G. Bihlmayer, A. Kubetzka, O. Pietzsch, S. Blügel, and R. Wiesendanger, Chiral magnetic order at surfaces driven by inversiona symmetry, Nature (London) **447**, 190 (2007).

[26] W. Eerenstein, N. D. Mathur, and J. F. Scott, Multiferroic and magnetoelectric materials, Nature (London) **442**, 759 (2006).

[27] J. M. Rondinelli, M. Stengel, and N. A. Spaldin, Carrier-mediated magnetoelectricity in complex oxide heterostructures, Nat. Nanotechnol. **3**, 46 (2008).

[28] C. L. Jia, A. Sukhov, P. P. Horley, and J. Berakdar, Piezoelectric control of the magnetic anisotropy via interface strain coupling in a composite multiferroic structure, Europhys. Lett. **99**, 17004 (2012).

[29] C. L. Jia, T. L. Wei, C. J. Jiang, D. S. Xue, A. Sukhov, and J. Berakdar, Mechanism of interfacial magnetoelectric coupling in composite multiferroics, Phys. Rev. B **90**, 054423 (2014).

[30] C. L. Jia, F. L. Wang, C. J. Jiang, J. Berakdar, and D. S. Xue, Electric tuning of magnetization dynamics and electric field-induced negative magnetic permeability in nanoscale composite multiferroics, Sci. Rep **5**, 11111 (2015).

[31] Y. J. Li, M. Chen, J. Berakdar, and C. L. Jia, Gate-controlled magnon-assisted switching of magnetization in ferroelectric/ferromagnetic junctions, Phys. Rev. B **96**, 054444 (2017).

[32] J. Bass and W. P. Pratt, Jr., Spin-diffusion lengths in metals and alloys, and spin-flipping at metal/metal interfaces: An experimentalist critical review, J. Phys.: Condens. Matter **19**, 183201 (2007).

[33] S. Chikazumi, *Physics of ferromagnetism* (Oxford University Press, New York, 2002).

[34] S. Sahoo, S. Polisetty, C.-G. Duan, S. S. Jaswal, E. Y. Tsymbal, and C. Binek, Ferroelectric control of magnetism in $BaTiO_3$/Fe heterostructures via interface strain coupling, Phys. Rev. B **76**, 092108 (2007).

[35] D. P. Landau, and K. Binder, *A guide to Monte Carlo simulations in statistical physics* (Cambridge University Press, New York, 2009).

[36] S. R. Etesami, A. Sukhov, and J. Berakdar, Kinetics of nanosize ferroelectrics, Phys. Rev. B **94**, 174105 (2016).

[37] G. Ederer and N. Spaldin, Effect of Epitaxial Strain on the Spontaneous Polarization of Thin Film Ferroelectrics, Phys. Rev. Lett. **95**, 257601 (2005).

[38] J. Hlinka and P. Mrton, Phenomenological model of a 90° domain wall in $BaTiO_3$-type ferroelectrics, Phys. Rev. B **74**, 104104 (2006).

[39] A. Sukhov, C. L. Jia, P. P. Horley, and J. Berakdar, Polarization and magnetization dynamics of a field-driven multiferroic structure, J. Phys.: Condens. Matter **22**, 352201 (2010).

[40] G. Venkataiah, Y. Shirahata, I. Suzuki, M. Itoh, and T. Taniyama, Strain-induced reversible and irreversible magnetization switching in $Fe/BaTiO_3$, J. Appl. Phys. **111**, 033921 (2012).

[41] J. B. Neaton, C. Ederer, U. V. Waghmare, N. A. Spaldin, and K. M. Rabe, First-principles study of spontaneous polarization in multiferroic $BiFeO_3$, Phys. Rev. B **71**, 014113 (2005).

[42] J. M. D. Coey, *Magnetism and magnetic materials* (Cambridge University Press, Cambridge, 2010).

[43] *Physics of ferroelectrics: A modern perpective*, edited by K. Rabe, Ch. H. Ahn, and J.-M. Triscone (Springer, Berlin, 2007).

[44] S. D. Yi, S. Onoda, N. Nagaosa, and J. H. Han, Skyrmions and anomalous Hall effect in a Dzyaloshinskii-Moriya spiral magnet, Phys. Rev. B **80**, 054416 (2009).

[45] J. Iwasaki, M. Mochizuki, and N. Nagaosa, Universal current-velocity relation of skyrmion motion in chiral magnets, Nat. Commun. **4**, 1463 (2013).

[46] N. Jedrecy, H. J. von Bardeleben, V. Badjeck, D. Demaille, D. Stanescu, H. Magnan, and A. Barbier, Strong magnetoelectric coupling in multiferroic $Co/BaTiO_3$ thin films, Phys. Rev. B **88**, 121409(R) (2013).

[47] C. Zhang, F. L. Wang, C. H. Dong, C. X. Gao, C. L. Jia, and C. J. Jiang, and D. S. Xue, Electric field mediated non-volatile tuning magnetism at the single-crystalline $Fe/Pb(Mg_{1/3}Nb_{2/3})_{0.7}Ti_{0.3}O_3$ interface, Nanoscale **7**, 4187 (2015).

[48] M. Mochizuki, Spin-Wave Modes and Their Intense Excitation Effects in Skyrmion Crystals, Phys. Rev. Lett. **108**, 017601 (2012).

[49] Y. Onose, Y. Okamura, S. Seki, S. Ishiwata, and Y. Tokura, Observation of Magnetic Excitations of Skyrmion Crystal in a Helimagnetic Insulator $Cu_2OSeO_3$, Phys. Rev. Lett. **109**, 037603 (2012).